

RF Magnetron Sputtered LiCoPO₄ Cathodes for 4.8V Thin Film Batteries

W. C. West,* J. F. Whitacre, and B. V. Ratnakumar

*Electrochemical Technologies Group
Jet Propulsion Laboratory
California Institute of Technology
Pasadena, CA 91109*

*email: william.c.west@jpl.nasa.gov

ABSTRACT

Thin film batteries employing sputtered LiCoPO_4 cathode layers, $\text{Li}_{3.3}\text{PO}_{3.8}\text{N}_{0.22}$ (LiPON) electrolyte and Li anode films have been successfully fabricated and tested. The cells exhibit a high voltage charge/discharge plateau of 4.8V, with a lower plateau at 2.5V corresponding to a much higher conductivity phase. Thin film batteries with as-deposited cathode layers are highly resistive and cannot be charged or discharged to appreciable capacities even at very low rates of approximately C/100. Upon annealing, the films sputtered from the LiCoPO_4 target become discontinuous and take on a granular structure. These grains are well indexed to untextured crystalline LiCoPO_4 on the Pt current collector, a finding further supported by the results from the electrochemical analyses. The thin film cells show no appreciable capacity fade or change in charge/discharge performance with increasing cycle number. The thin film cells employing the fully crystalline LiCoPO_4 are among the highest voltage thin film batteries yet reported.

INTRODUCTION

The driving forces behind the development of improved thin film batteries are markedly different compared with those for conventional batteries. For example, whereas gravimetric and volumetric energy densities (in units of Wh/g and Wh/l, respectively) are of critical importance for comparing battery performance for conventional batteries, these quantities are of much lesser importance for thin film batteries, where in many cases the substrate and encapsulation layer mass and volume can far exceed the mass and volume of the battery active materials. A metric that is of primary importance for thin film

batteries relates to specific energy per unit area, which can be affected by several variables related to the cell design. The amount of active electrode thickness that can be both deposited and successfully adhered to a current collector affects the specific energy per unit area. For typical anode-heavy Li thin film batteries of the design set forth by the Oak Ridge National Laboratories (ORNL) group¹, a sputtered cathode film of LiCoO₂ with thickness beyond 5 μm becomes difficult to achieve due to cracking and poor adhesion. Constrained by the practical limit of the thickness that can be deposited in a reasonable amount of time, with good adhesion and electrochemical accessibility, one must look to other factors that can enhance areal specific energy beyond simply increasing the cell thickness or footprint.

Another approach for improving areal specific energy is to increase the cell voltage through selection of alternate cathode layers with redox potentials higher than the state-of-the-art sputtered LiCoO₂. Several candidate materials have been reported in the literature or are currently being studied. The spinel LiMn₂O₄ system has shown significant promise upon partial substitution of Mn with other metallic atoms, such as Co, Mg, Fe, Ni, Fe, Al, Ti, or Zn.² The substitutional atoms serve to stabilize the spinel structure to allow for extended cycling, and can also add a second discharge plateau of higher potential than the nominally 4V Mn²⁺/Mn³⁺ redox couple. Of these, the LiMn_{1.5}Ni_{0.5}O₄ system was found to have the best stability, delivering up to 130 mAh/g at a relatively high 4.7V.³ A number of studies have been conducted on LiMn₂O₄ deposited as thin films by electron-beam evaporation, sputter deposition, chemical vapor deposition (CVD), and pulsed laser deposition (PLD).⁴⁻⁷ These works were generally successful in creating functional polycrystalline or nanocrystalline thin films of LiMn₂O₄, despite the

fact that this materials system is notoriously sensitive to processing conditions due to the existence of a host of defect spinels. Additionally, a charge plateau in excess of 5V was reported for sputter-deposited LiMn_2O_4 , though overcharging these cells to greater than 4.5V was found to significantly decrease cycle life, and a strong 5V discharge plateau was not observed.⁴ In addition, a study of sputter deposited substitutional $\text{Li}_y\text{Mn}_x\text{Ni}_{2-x}\text{O}_4$ has been successfully conducted in our labs and will be published separately.⁸

Recently, the class of compounds known as phospho-olivines has attracted attention as conventional rechargeable Li-ion battery electrodes. LiFePO_4 has good theoretical specific capacity of 170 mAh/g, though the poor electronic conductivity has limited the practical specific capacity to roughly 110 mAh/g.⁹ To address the issue of poor conductivity, other groups have either modified the synthesis route to coat the LiFePO_4 particles with carbon,¹⁰ or have doped the LiFePO_4 with metals superionic to Li.¹¹

Aside from the cost benefits and good capacity of LiFePO_4 , a drawback of the compound is that the cathode potential versus lithium is only 3.5V, which does not compare favorably to LiCoO_2 at 4V. However, conventional cells (with liquid electrolyte) employing olivine LiCoPO_4 as the active cathode material have been very recently reported to have an outstanding cell voltage of 4.8 – 5V.¹²⁻¹⁴ Thus, a study was performed to attempt to fabricate solid state thin film batteries employing this attractive cathode materials system in place of the much more commonly used sputtered LiCoO_2 films. But the difficulties encountered in preparing RF magnetron sputtered ceramic films, particularly from materials with polyanions, are non-trivial. Sputtering can be considered an atomic level process and though polyatomic clusters can be ejected from

the target material, disproportionation of the sputtered species due to varying sputter yield is typical. In this article, we report for the first time the successful fabrication of thin film batteries using sputter deposited LiCoPO_4 that have charge/discharge plateaus of 4.8V and are capable of multiple charge/discharge cycles.

EXPERIMENTAL

All solid-state thin film battery cells were fabricated on silicon nitride coated single crystal silicon substrates. The deposition of all the films (except the anode layer) was carried out in a planar, three target RF magnetron sputtering chamber, evacuated to a base pressure of less than 2×10^{-6} Torr with a turbomolecular pumping system. The first layer consisted of a Ti adhesion layer and Pt current collector that was patterned through a shadow mask. The LiCoPO_4 layer was then sputtered onto the cathode current collector, and in some cases, then annealed to various temperatures in air. Next, the solid electrolyte film of $\text{Li}_{3.3}\text{PO}_{3.8}\text{N}_{0.22}$ (LiPON) was deposited onto the cathode layer by sputtering a Li_3PO_4 target in N_2 , after Yu *et al.*¹⁵ Finally, a Li metal anode layer was thermally evaporated onto the electrolyte through a second shadow mask to complete the cell. The deposition parameters for the layers are listed in Table 1.

The LiCoPO_4 target was fabricated using a solid-state synthesis process. Stoichiometric amounts Co_3O_4 (J. T. Baker), $(\text{NH}_4)_2\text{HPO}_4$ (J. T. Baker), and Li_2CO_3 (Alfa Aesar) were mixed and heated slowly to 350°C for 16 hours, ground and remixed, then heated at 350°C for 6 more hours. The mixture was then heated to 750°C for 24 hours, ground and remixed. The resultant powder was mixed with a 1% solution of ethylene propylene diene monomer (EPDM) binder in cyclohexane. The suspension was gently heated to drive off the solvent, and the powder was then pressed at 2800 psi to

form a 3" diameter, ¼" thick pellet. The pellet was then heated to 300°C for 1 hour and ramped to 750°C for 24 hours. After cooling, the LiCoPO₄ pellet was mounted onto an Al backing plate with conductive Ag epoxy. The target material characterized using a Siemens D500 diffractometer run in the theta - 2 theta geometry, with a Cu anode at an accelerating voltage of 40 kV and a tube current of 20 mA.

Film crystallography and microstructure characterization was performed at the Stanford Synchrotron Radiation Laboratory (SSRL). A synchrotron x-ray source was used because these thin (typically < 0.3 μm), low atomic weight films yielded poor counting statistics using laboratory-based x-ray diffraction systems. To maximize the scattered signal, the asymmetric GIXS geometry was used on beamline 2-1 at SSRL (3 GeV and 100 mA at fill).¹⁶ A silicon (111) monochromator was used to select the wavelength of the x-ray beam, 0.154996 nm, in focused mode. The vertical and horizontal divergences of the beam were 0.2 mrad and 3 mrad, respectively. Slits 1 x 1 mm in area were used to define the incident beam and a second Si(111) monochromator was used on the detector arm. Diffracted x-ray intensity was measured using a standard scintillation counter. Samples were manipulated using an automated Hüber two-circle diffractometer that was controlled using a UNIX workstation. The incident beam dose was measured by a scintillation detector placed upstream, off of a beam-splitter, from the incident beam slits. The samples were kept dry in vacuum-pumped pouches during transport to SSRL. All measurements were conducted using a set dose for each data point, eliminating any possible experimental error due to beam intensity fluctuation.

To quantify the Li/Co ratio in the LiCoPO₄ films, an HP 4500 inductively coupled plasma-mass spectrometer (ICP-MS) station was employed, using a set of NIST –

traceable Co/Li calibration standards (with Li/Co ratios ranging from 0.75 to 1.25). Analytical samples were prepared by digesting the films in concentrated HNO₃, followed by dilution in deionized water. To avoid detector non-linearity issues, the Li and Co concentrations in the standards were set to similar levels as those observed in the samples. Surface morphology was studied using a Hitachi field-emission scanning electron microscope (SEM).

The electrochemical characterization of the films was performed using a Solartron 1286 frequency response analyzer and a Princeton Applied Research 273A potentiostat, driven by Zplot and Corrware Software (Scribner Associates). Cyclic voltammetry measurements were performed with sweep rates between 0.1 – 5 mV/s. The applied AC signal for the electrochemical impedance spectroscopy (EIS) measurements was 40 mV, with frequency between 65000 – 0.5 Hz. The EIS data was fitted to equivalent circuit models by a complex least square fitting program, Zview (Scribner Associates).

RESULTS AND DISCUSSION

Materials Characterization

The target material was confirmed by x-ray diffraction to be pristine orthorhombic LiCoPO₄, as shown in Fig. 1. The thin films deposited onto the Pt current collectors by sputtering the LiCoPO₄ target were visually smooth and featureless. Upon annealing, these films roughened with increasing annealing temperature. SEM studies indicated that with increasing annealing temperature, the deposited film transitioned from a mottled yet contiguous surface to disconnected islands of granular material, to a surface of individual grains of crystallites (Fig. 2). These crystallites are clearly visible in the

SEM micrographs in Fig. 3B for the 700°C annealed samples, where the grains grow via an Ostwald ripening mechanism suggested by Fig. 3A at the 500°C annealed samples.

Synchrotron x-ray diffraction measurements show that as-deposited films sputtered from the LiCoPO₄ target were fully amorphous, with the only diffraction peaks observed resulting from the Pt current collector. For samples annealed in air for one hour at 300°C, no diffraction peaks aside from the Pt layer were discerned, as well. However, films that were annealed at 700°C for one hour showed sharp reflections that are well indexed to the LiCoPO₄ olivine structure (Fig. 4). It is interesting to note that these films do not exhibit any appreciable texturing based on a qualitative examination of expected relative intensities. This result contrasts with typical sputtered and annealed films (e.g. LiCoO₂)^{17, 18} which are usually highly textured as a consequence of residual stress imparted by the sputter deposition process. Whereas the SEM micrographs of the 700°C annealed layers indicated that the feature size of the crystallites was about 1 μm in diameter, the average crystal grain size was calculated to be 100 ± 20 nm from the Scherrer formula. Thus the particles visible in the SEM micrographs were quite likely polycrystalline.

ICP-MS data showed that the films, as sampled from multiple areas from the same substrate had a Li/Co ratio of 0.95 ± 0.1. This value was within error of the expected 1:1 stoichiometry, though it is common for sputtered films of Li-bearing ceramics such as LiCoO₂ to be slightly lithium deficient, given the low sputter yield of Li relative to the other target elements, and due to rapid diffusion of Li away from the target erosion ring during sputtering.^{19, 20}

Electrochemical Cell Results

After deposition of the LiCoPO_4 on Pt current collectors (followed in some cases by an annealing step), the substrates were coated with sputtered films of LiPON, and evaporated Li metal anodes to fabricate thin film battery cells. Because the deposited LiCoPO_4 layers after annealing were not a uniform film but rather a layer of crystallites, care must be used in interpreting electrochemical results; current densities for example, cannot be accurately estimated and thus cell data were reported in terms of layer thickness and area prior to anneal or in terms of C-rates.

The cells fabricated using an as-deposited LiCoPO_4 cathode film were highly resistive and could not be charged or discharged at even very low C-rates, on the order of C/100. Cells that were annealed for one hour at 700°C had dramatically improved performance, with single high voltage charge/discharge plateau at about 4.8V (Fig. 5). The cell capacity at C/110 was measured to be $11 \mu\text{A}\cdot\text{hr}/\mu\text{m}\cdot\text{cm}^2$, based on an active cell area of 0.48 cm^2 and a cathode thickness of $0.285 \mu\text{m}$ prior to annealing. This cathode capacity value is low relative to state-of-the-art sputtered and annealed LiCoO_2 films which typically afford areal specific capacity values of $69 \mu\text{A}\cdot\text{hr}/\mu\text{m}\cdot\text{cm}^2$ at 3.9V.²¹ Although others have reported that the capacity of LiFePO_4 can be improved by slightly elevating the cell temperature to ca. 55°C ,²² no attempts were made in this study to charge and discharge the thin film cells at elevated temperature.

The rate capability of the cells is shown in Fig. 6; a weak relationship is found between cell voltage and capacity. The thin film cells employing the LiCoPO_4 cathodes have no significant capacity fade with cycling, as shown in Fig. 7, over at least the first

few tens of cycles. Further cycle life studies are currently underway to better estimate the capacity fade with cycling.

The observation that the cell voltage is a weak function of capacity (or more precisely, Li content) is consistent with that observed for other phospho-olivine cathode studies that contend multiple phases are present in the cathode. In principle, the cathode voltage (relative to Li) is constant when two electrochemically active phases are present, by Gibb's Phase Rule. Padhi *et al.*⁹ demonstrated that chemically delithiating LiFePO_4 did not simply remove the Li from the LiFePO_4 lattice to yield fractional Li/Fe ratios, but rather resulted in the appearance of a second phase, indexed as FePO_4 . Amine *et al.*¹² reported x-ray diffraction results for bulk LiCoPO_4 electrode powders before and after charge that were interpreted as evidence for two phases present.

It is a reasonable assumption based on the above references that a fully delithiated cobalt phosphate phase appears at the expense of stoichiometric LiCoPO_4 during charging. For LiFePO_4 , delithiation to FePO_4 does not induce large changes in the crystalline structure; both compounds are of the same space group (Pbnm), and the volume of the unit cell decreases by 6.81% and the density decreases by 2.59%.⁹ In contrast, CoPO_4 has not been described in literature. The monoclinic $\text{Co}_3(\text{PO}_4)_2$ is a possible species resulting from delithiation of orthorhombic LiCoPO_4 . However, the $\text{Co}_3(\text{PO}_4)_2$ unit cell volume and density are 12.4% and 1.4% greater, respectively, than that of LiCoPO_4 . Large dilations and contractions in the cell volume during charging and discharging may ultimately limit the cathode cycle life. No synchrotron diffraction data from sputtered LiCoPO_4 cathodes at delithiated states has been collected to date, though this experiment is planned and results will be presented at a later date.

A curious feature of the cell performance is observed at cell voltages near 2.5V. As fabricated in the discharged state, the open circuit voltage was typically observed to be roughly 2.0V. Upon charge, the cell voltage plateaus at 2.5V even at 1C charging rate, which is significantly higher rate than can be accommodated at the 4.8V plateau (Fig. 8). This low voltage plateau is present on discharge and does not fade with cycling. Cyclic voltammetry measurements (Fig. 9) show that the anodic and cathodic peaks associated with the 2.5V plateau are narrower and less widely spaced than the 5V - 4.6V complementary peaks. The origin of this more conductive state at cell voltage of 2.5V is not understood at this time. Typically, published reports of conventional liquid electrolyte phospho-olivine based cells do not cycle below 3V, so whether this low voltage plateau is common to LiCoPO_4 cathodes prepared by more conventional means is not known.

EIS studies independently verify the presence of this more conductive low voltage regime. Bode plots of the full cells as a function of open circuit voltage are shown in Figs. 10 and 11. From equivalent circuit modeling, the cathode layer resistance reaches a minimum at 2.5V, and rises with increasing cell voltage until approximately 3.3V (Fig. 12). Above this voltage, the model becomes quite insensitive to cathode impedance, and thus cannot accurately predict the cathode impedance terms. Given the discontinuity of the cathode layer on the current collector, conventional equivalent circuit models representing thin film battery cells cannot be used. Thus, the equivalent circuit model bears a brief discussion.

The starting point for the analysis of the equivalent circuit model is one representing a Pt|LiPON|Li cell. This model was described by Yu *et al.*,¹⁵ and is shown

in Fig. 13A. The electrolyte may be represented by a constant phase element $CPE_{(el)}$ in parallel to an electrolyte resistance $R_{(el)}$, where the impedance $Z_{(CPE)}$ is given by:

$$Z_{(CPE)} = A(j\omega)^{-\alpha} \quad [1]$$

The fitting parameters were A and α , $j = (-1)^{1/2}$, and $\omega = 2\pi f$.

The electrolyte is in series with a reaction layer term represented by a $CPE_{(rxn)}$ in parallel to a reaction resistance $R_{(rxn)}$. A geometric capacitance term is placed in parallel to these two elements, which is then in series with an interfacial term $CPE_{(int)}$. This model was fitted to the test cells of the form Pt|LiPON|Li fabricated in this study. The next step calls for including the cathode layer in this model. For a cathode layer that completely covers the Pt current collector, a constant phase element and a parallel resistor would be placed in series to the electrolyte and reaction layer elements, all in parallel to the geometric capacitance. However, since the cathode layers fabricated in this study are granular in nature and not contiguous, this approach is inaccurate. The model is more accurately described by placing the cathode elements in parallel to the reaction layer and in series to the electrolyte terms (Fig. 13B). The fitting parameters are shown in Table 2.

The efficacy of the model is apparent when comparing the impedance spectra of the amorphous cathode cells and the annealed cathode cells. Unlike the annealed cathode cells, the unannealed cathode films completely cover the current collector and therefore cannot be modeled with the cathode constant phase element and resistor in parallel to the reaction layer terms. Whereas a significant relaxation appears at roughly 500 Hz for the annealed cathode cells regardless of cell voltage, no relaxation is apparent for the unannealed cathode cells (Fig. 14). Although the unannealed cathode cells have higher impedances at all frequencies measured relative to the annealed cathode cells, the

different impedance spectra characteristics cannot be simply attributed to higher cathode resistance. The model shown in Fig. 13B predicts that for cathode resistances beyond approximately $10^6 \Omega$, there will be no change in the impedance spectra profile.

CONCLUSIONS

Thin film batteries employing sputtered LiCoPO_4 layers have been successfully fabricated and tested in terms of cathode structural and morphological properties, and electrochemical performance. The cells exhibit a high voltage charge/discharge plateau of 4.8V, with a much lower plateau at 2.5V corresponding to a much higher conductivity phase. Thin film batteries with as-deposited cathode layers are highly resistive and cannot be charged or discharged to appreciable capacities even at very low rates of C/100. Upon annealing the films sputtered from the LiCoPO_4 target, the films become discontinuous and take on a granular structure. These grains are well indexed to untextured crystalline LiCoPO_4 on Pt. The impedance spectra of the cells have been fitted using an equivalent circuit model that takes into account the discontinuous nature of the cathode layer. From the impedance spectra fitting, it is shown that the resistance of the cathode layer increases with open circuit voltage. The annealed thin film cells show no appreciable capacity fade or change in charge/discharge performance with increasing cycle number. The thin film cells employing the fully crystalline LiCoPO_4 are among the highest voltage thin film batteries yet reported.

ACKNOWLEDGEMENTS

This work was carried out at the Jet Propulsion Laboratory, California Institute of Technology, under contract with the National Aeronautics and Space Administration. The authors would like to thank H. Rockstad preparing the silicon nitride films, J. Kulleck for performing the Siemens x-ray diffraction measurements, and S. Surampudi for providing guidance throughout the project.

REFERENCES

- ¹See for example: J. B. Bates, N. J. Dudney, B. Neudecker, A. Ueda, and C. D. Evans, *Solid State Ionics*, **135**, 33 (2000).
- ²X. Wu, and S.B. Kim, *J. Power Sources*, **109** 53 (2002).
- ³K. Amine, H. Tukamoto, H. Yasuda, and Y. Fujita, *J Power Sources*, **68**, 604 (1997).
- ⁴J. B. Bates, D. Lubben, N. J. Dudney, and F. X. Hart, *J. Electrochem. Soc.*, **142**, L149 (1995).
- ⁵N. J. Dudney, J. B. Bates, R. A. Zuhr, S. Young, J. D. Robertson, H. P. Jun, and S. A. Hackney, *J. Electrochem. Soc.*, **146**, 2455 (1999).
- ⁶P. Fragnaud, R. Nagarajan, D. M. Schleich, and D. Vujic, *J. Power Sources*, **54**, 362 (1995).
- ⁷K. A. Striebel, C. Z. Deng, S. J. Wen, and E. J. Cairns, *J. Electrochem. Soc.*, **143**, 1821 (1996).
- ⁸J. F. Whitacre, W. C. West, and B. V. Ratnakumar, submitted to *J. Electrochem. Soc.*, January 2003.
- ⁹A. K. Padhi, K. S. Najundaswamy, and J. B. Goodenough, *J. Electrochem. Soc.*, **144**, 1188 (1997).
- ¹⁰Z. H. Chen, and J. R. Dahn, *J. Electrochem. Soc.*, **149**, A1184 (2002); S. Franger, F. Le Cras, C. Bourbon, and H. Rouault, *Electrochem. Solid State Lett.*, **5**, A231 (2002); S. F. Yang, Y. N. Song, P. Y. Zavalij, and M. S. Whittingham, *Electrochem. Comm.*, **4**, 239 (2002); P. P. Prosini, D. Zane, and M. Pasquali, *Electrochem. Acta*, **46**, 3517 (2001); H. Huang, S. C. Yin, and L. F. Nazar, *Electrochem. Solid State Lett.*, **4**, A170 (2001).
- ¹¹S.-Y. Chung, J. T. Bloking, and Y.-T. Chiang, *Nature Materials*, **1**, 123 (2002).
- ¹²K. Amine, H. Yasuda, and M. Yamachi, *Electrochem. Solid State Lett.*, **3**, 178 (2000).
- ¹³S. Okada, S. Sawa, M. Egashira, J.-I. Yamaki, M. Tabuchi, H. Kageyama, T. Konishi, and A. Yoshino, *J. Power Sources*, **97-98**, 430 (2001).
- ¹⁴J. M. Lloris, C. P. Vicente, and J. L. Tirado, *Electrochem. Solid State Lett.*, **5**, A234 (2002).
- ¹⁵X. Yu, J. B. Bates, G. E. Jellison, and F. X. Hart, *J. Electrochem. Soc.*, **144**, 524 (1997).
- ¹⁶ http://smb.slac.stanford.edu/powder/#diffractometer_at_SSRL

- ¹⁷J.F. Whitacre, W.C. West, E. Brandon, and B.V. Ratnakumar, *J. Electrochem. Soc.*, **148**, A1078 (2001).
- ¹⁸J. B. Bates, N. J. Dudney, B. J. Neudecker, F. X. Hart, H. P. Jun, and S. A. Hackney, *J. Electrochem. Soc.*, **147**, 59 (2000).
- ¹⁹N. J. Dudney, J. B. Bates, R. A. Zuhr, and C. F. Luck, *Solid State Ionics*, **53-56**, 655 (1992).
- ²⁰J. F. Whitacre, W. C. West, and B. V. Ratnakumar, *J. Power Sources*, **103**, 134 (2001).
- ²¹B. Wang, J. B. Bates, F. X. Hart, B. C. Sales, R. A. Zuhr, and J. D. Robertson, *J. Electrochem. Soc.*, **143**, 3203 (1996).
- ²²S. Franger, F. Le Cras, C. Bourbon, and H. Rouault, *Electrochem. Solid State Lett.*, **5**, A231 (2002).

Figure captions:

- Fig. 1. X-ray diffraction pattern for the LiCoPO_4 sputter target. The indices for LiCoPO_4 are indicated below the diffraction pattern.
- Fig. 2. SEM micrographs at 200X of sputtered LiCoPO_4 on Pt/Ti. A) as-deposited film, B) annealed at 300°C for one hour, C) annealed at 500°C for one hour, D) annealed at 700°C for one hour
- Fig. 3. SEM micrographs at 1500X of sputtered LiCoPO_4 on Pt/Ti. A) annealed at 500°C for one hour, B) annealed at 700°C for one hour
- Fig. 4. Synchrotron x-ray diffraction patterns for sputtered LiCoPO_4 for three different samples: as deposited, after annealing at 300°C , and after annealing at 700°C for one hour. The diffraction data was not collected beyond a 2-theta angle of 27.5° since no well-defined diffraction peaks were collected up to this point.
- Fig. 5. Charge/discharge profile of a cell fabricated with a 700°C annealed LiCoPO_4 cathode. The cell was charged and discharged at a C/110 rate.
- Fig. 6. Discharge capacity of a cell fabricated with a 700°C annealed LiCoPO_4 cathode, as a function of voltage, at various C rates. All discharges followed a C/110 rate charging step.
- Fig. 7. Charge and discharge time as a function of cycle. This data was collected at the between the cell's 6th and 14th cycles.
- Fig. 8. A typical initial charge from the as-fabricated, discharged state. The charging rate for this cell was 1C.
- Fig. 9. Cyclic voltammetry scan for $\text{LiCoPO}_4|\text{LiPON}|\text{Li}$ cells at 0.1 mV/s.
- Fig. 10. Bode plots for $\text{LiCoPO}_4|\text{LiPON}|\text{Li}$ cells, open circuit voltage 2.2 – 2.8V.
- Fig. 11. Bode plots for $\text{LiCoPO}_4|\text{LiPON}|\text{Li}$ cells, open circuit voltage 3 - 3.6V.
- Fig. 12. Cathode layer resistance as a function of open circuit voltage, from EIS fitting data.
- Fig. 13. Equivalent circuit models. A) Pt|LiPON|Li cell, B) (Pt + LiCoPO_4)|LiPON|Li cell.
- Fig. 14. Complex plane plots of $\text{LiCoPO}_4|\text{LiPON}|\text{Li}$ cells, with unannealed and annealed cathode layers. The inset shows the plot details at lower impedances.

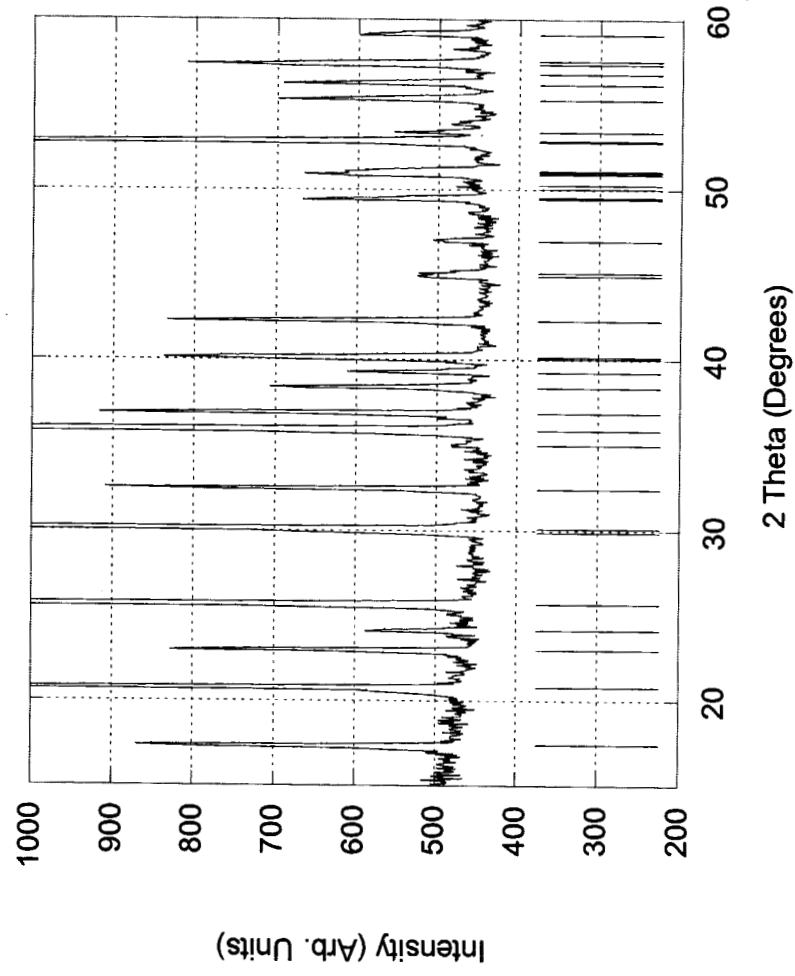


Fig. 1.

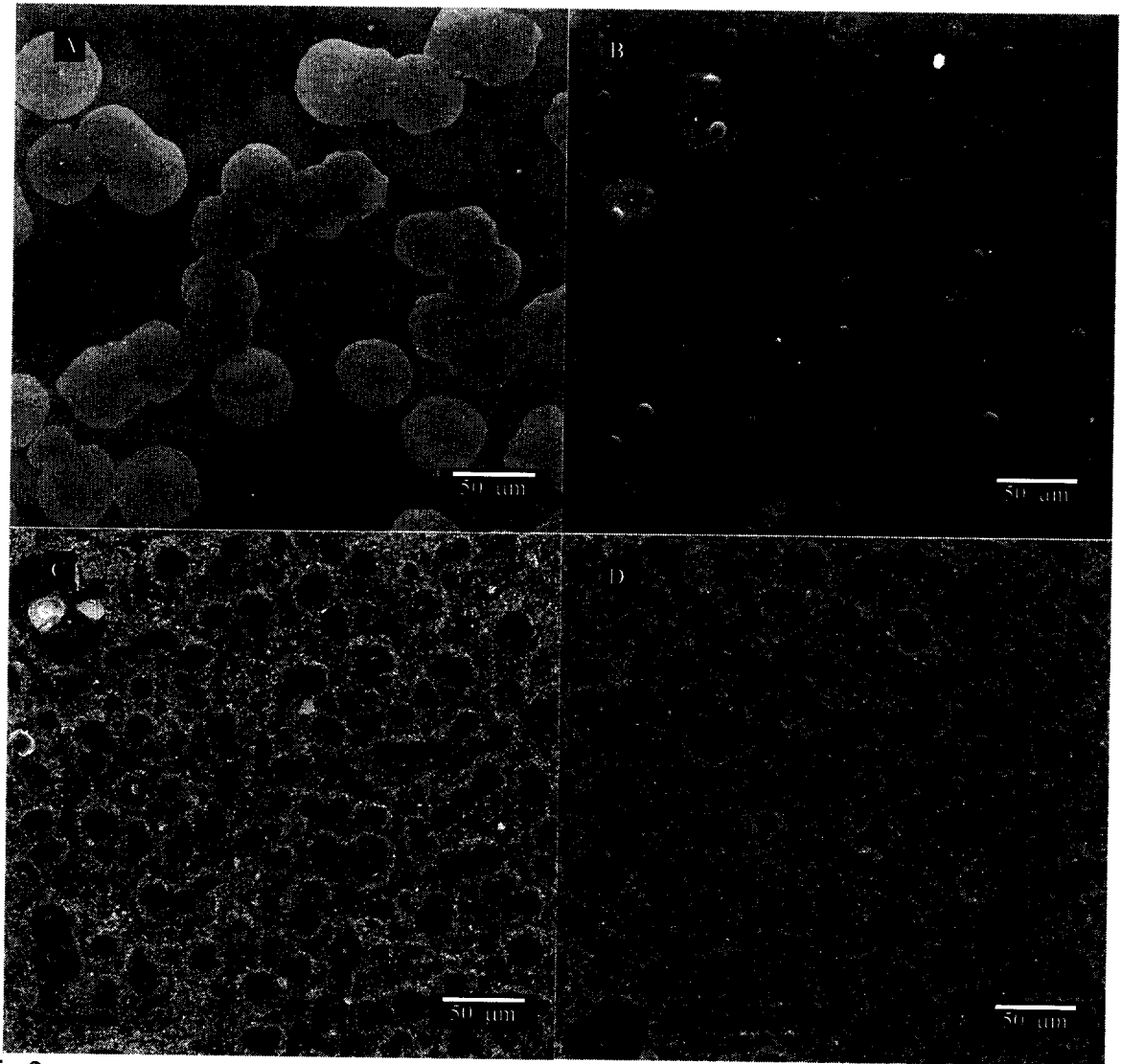


Fig 2.

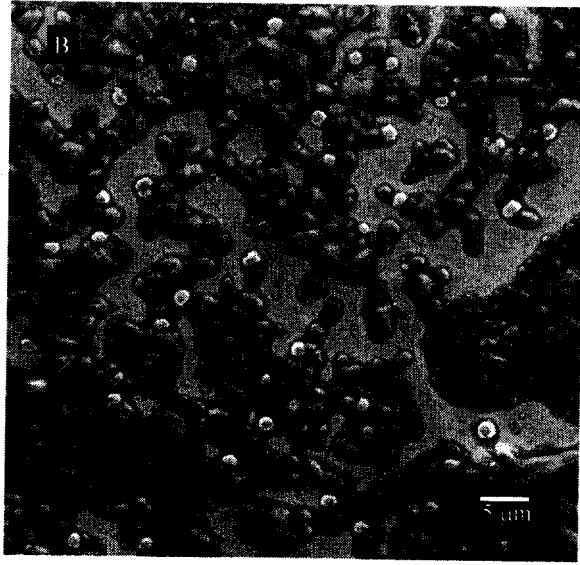
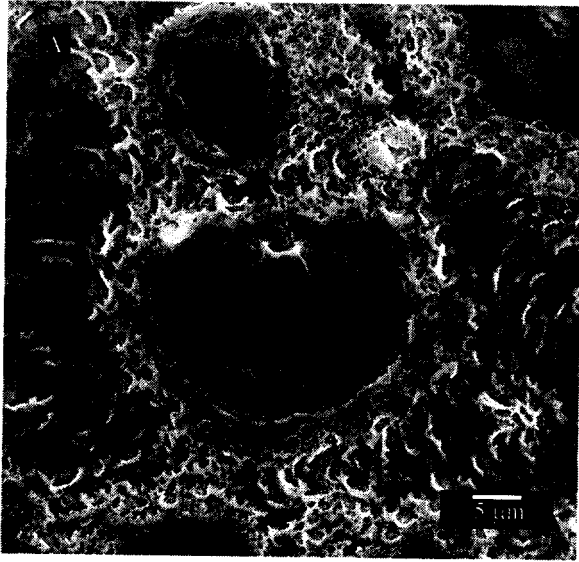


Fig.3.

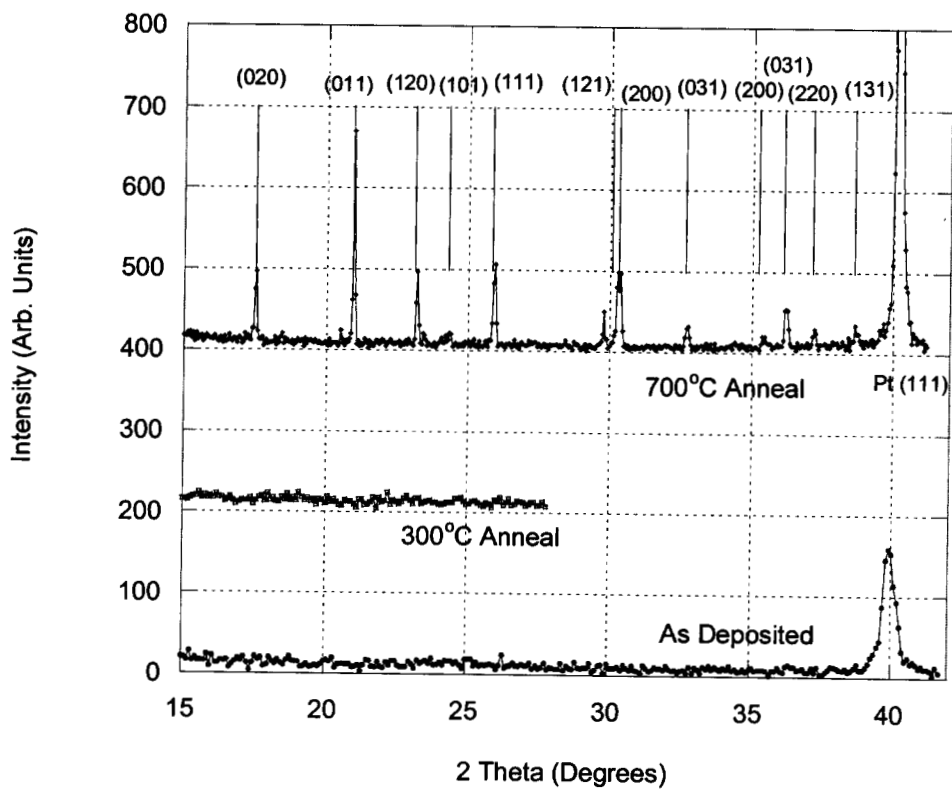


Fig. 4

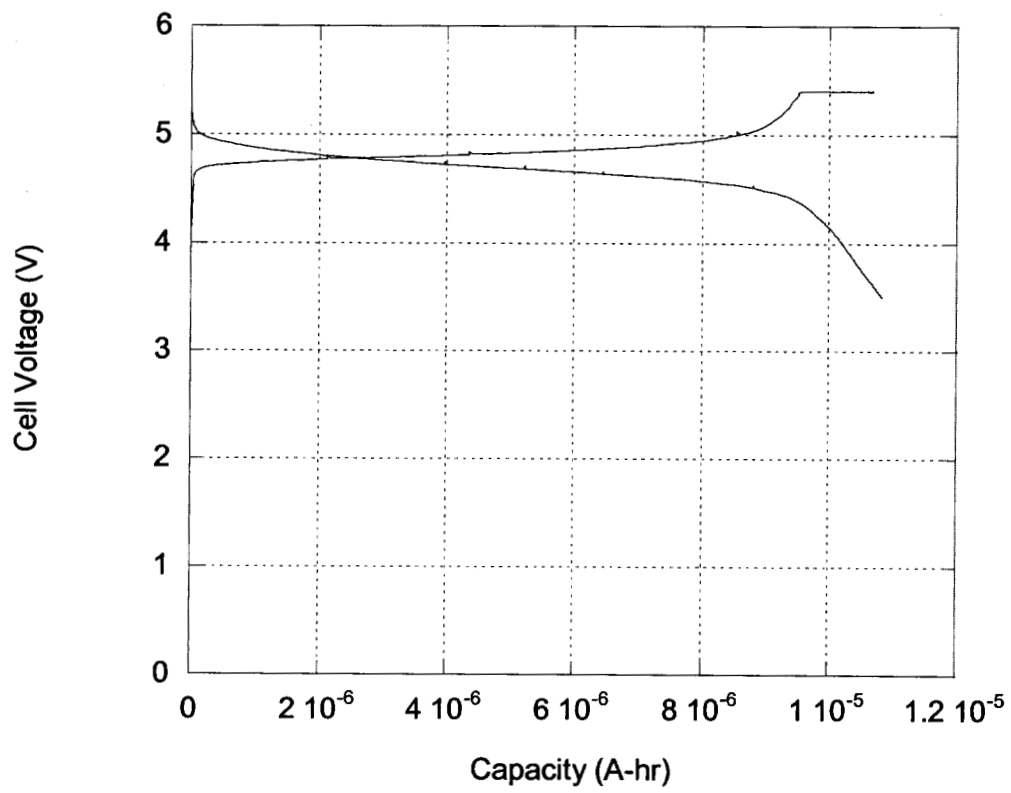


Fig. 5.

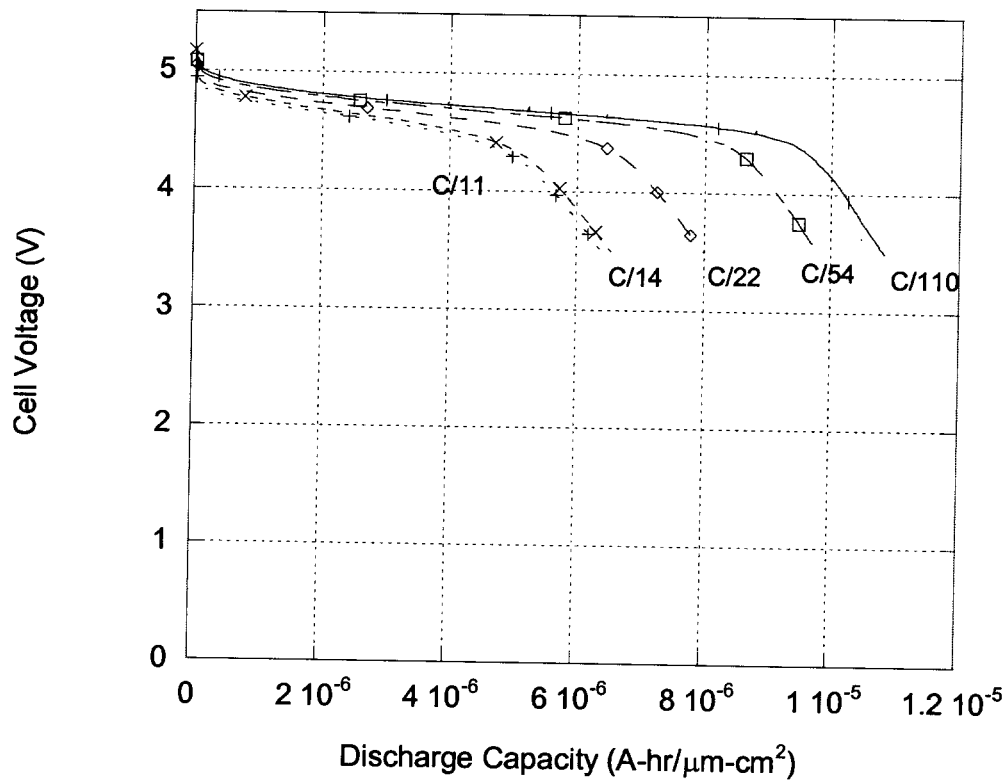


Fig. 6.

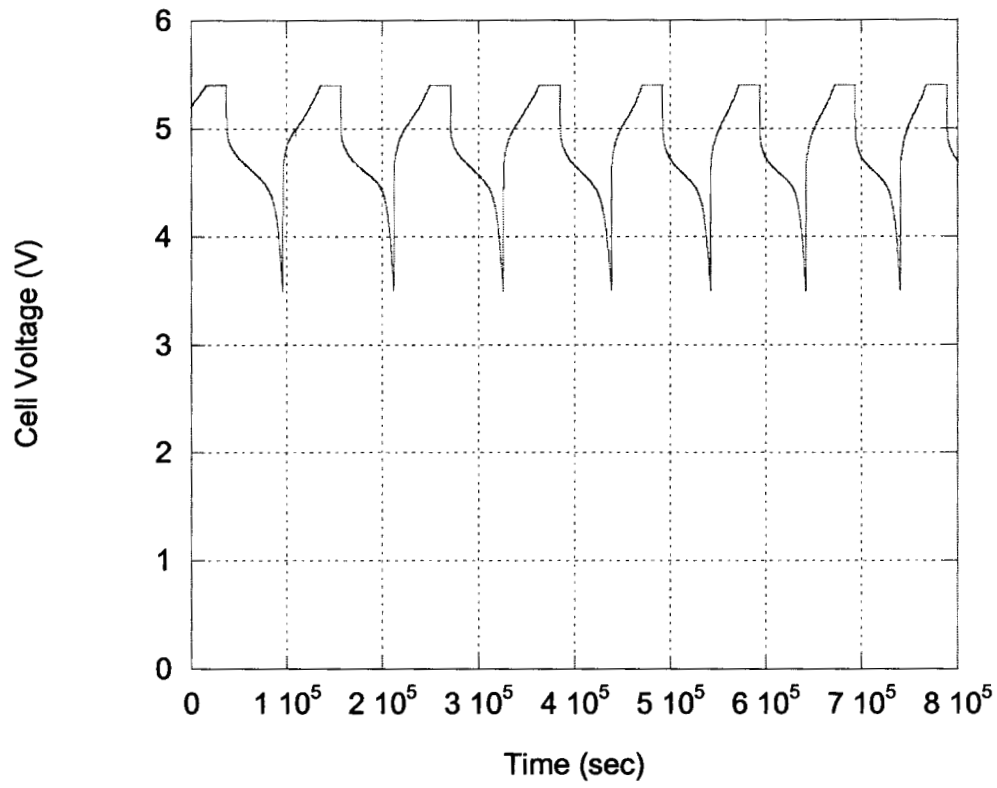


Fig. 7.

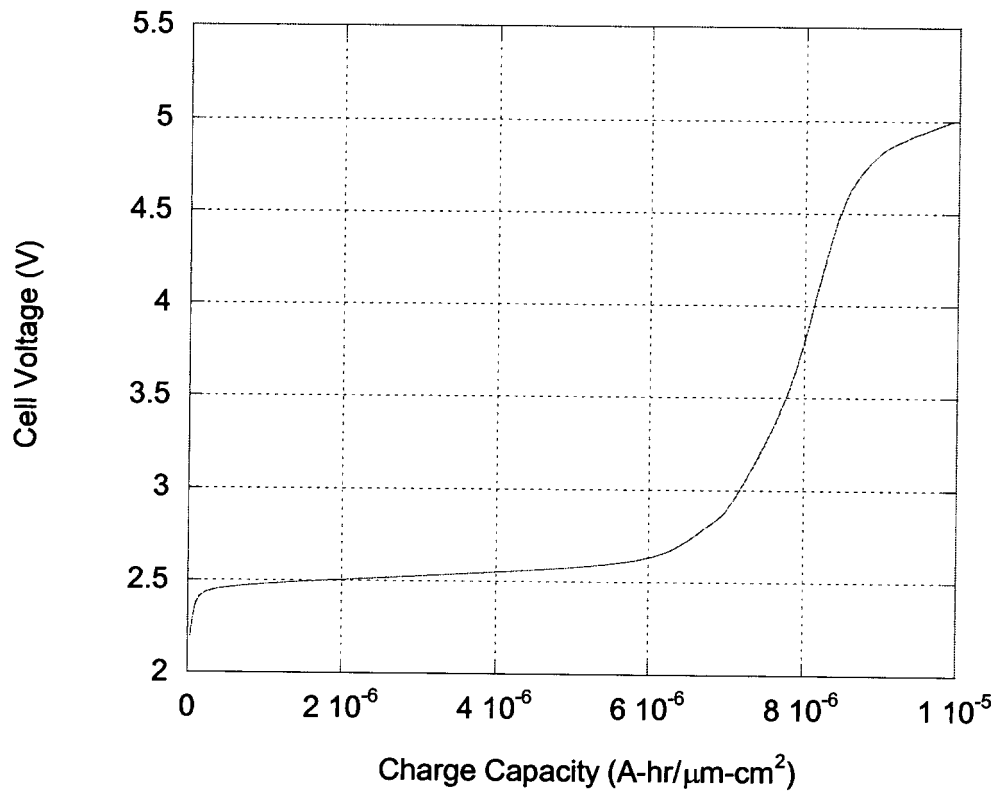


Fig. 8.

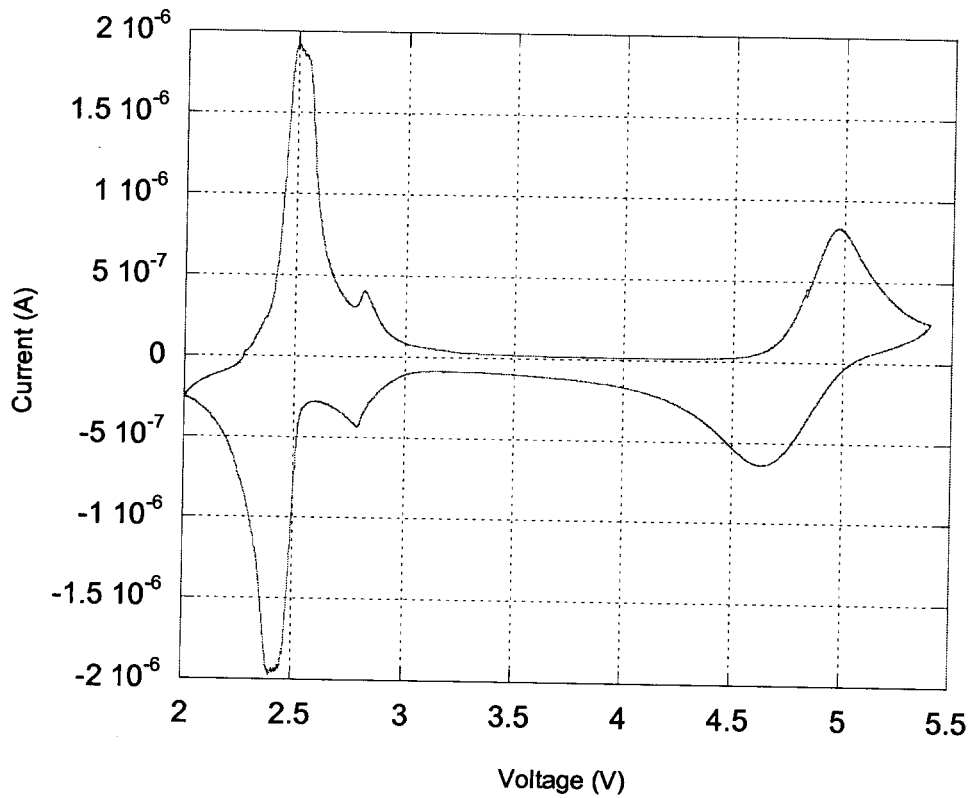


Fig. 9.

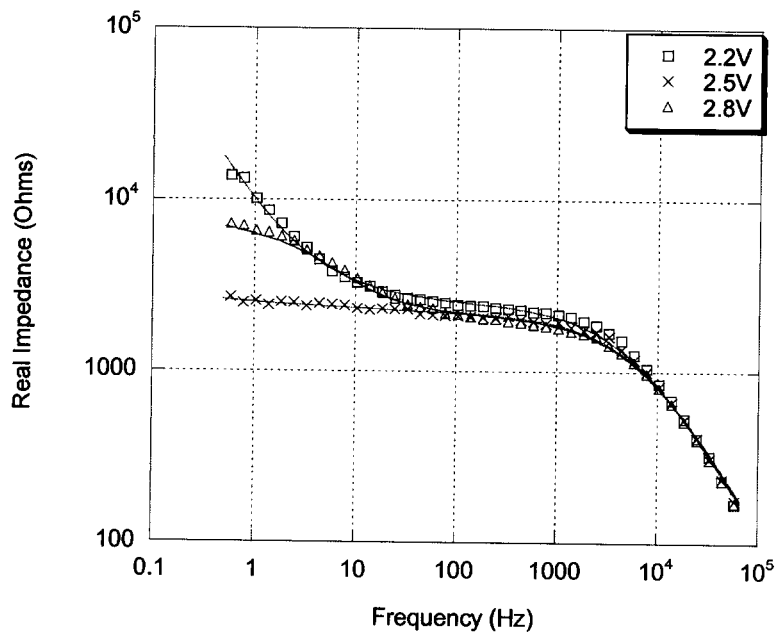
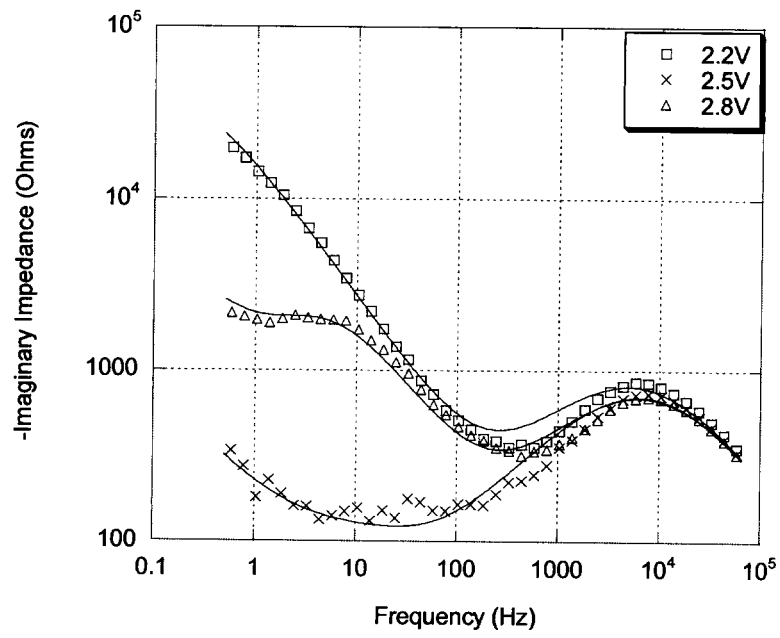


Fig. 10

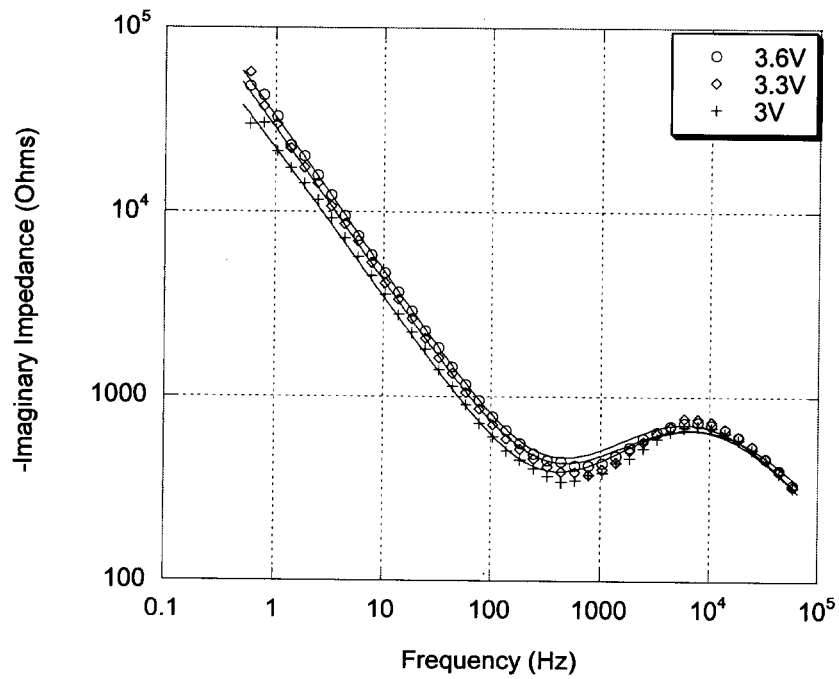
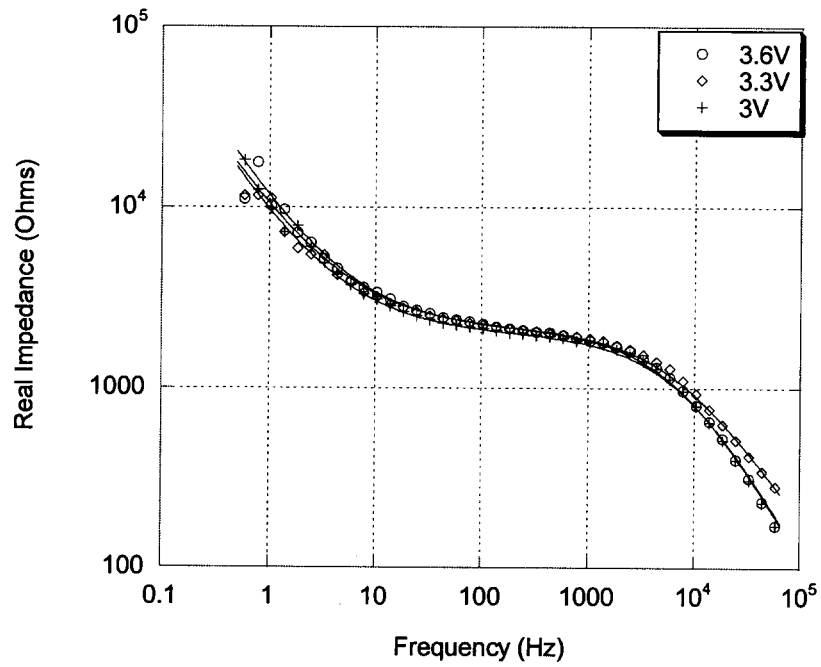


Fig. 11

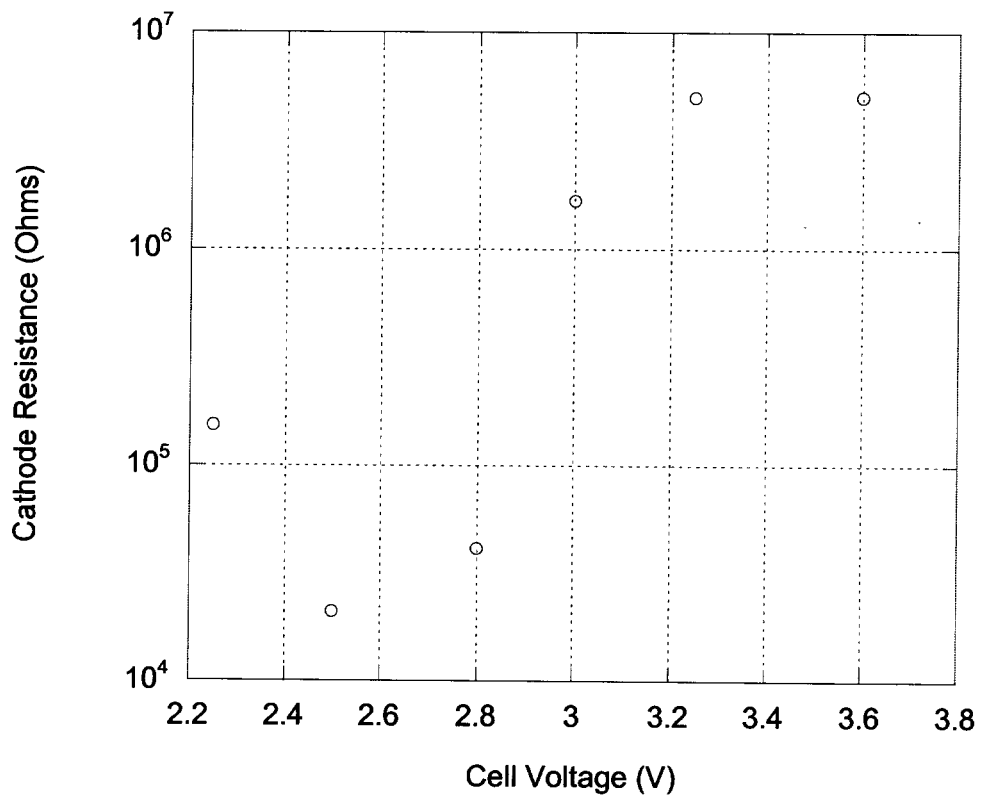
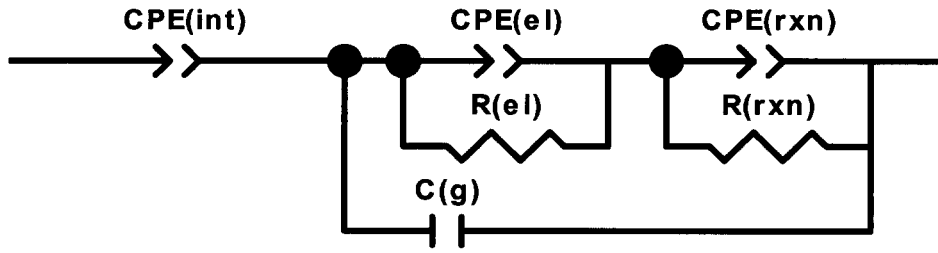


Fig. 12

A



B

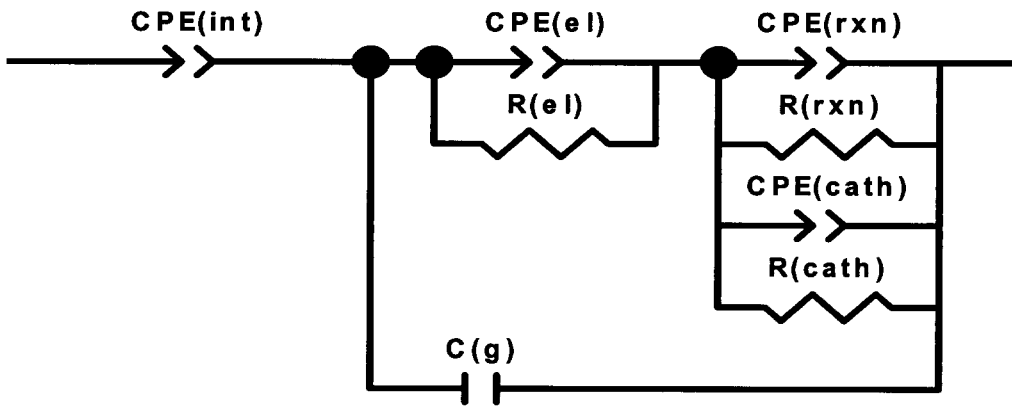


Fig. 13.

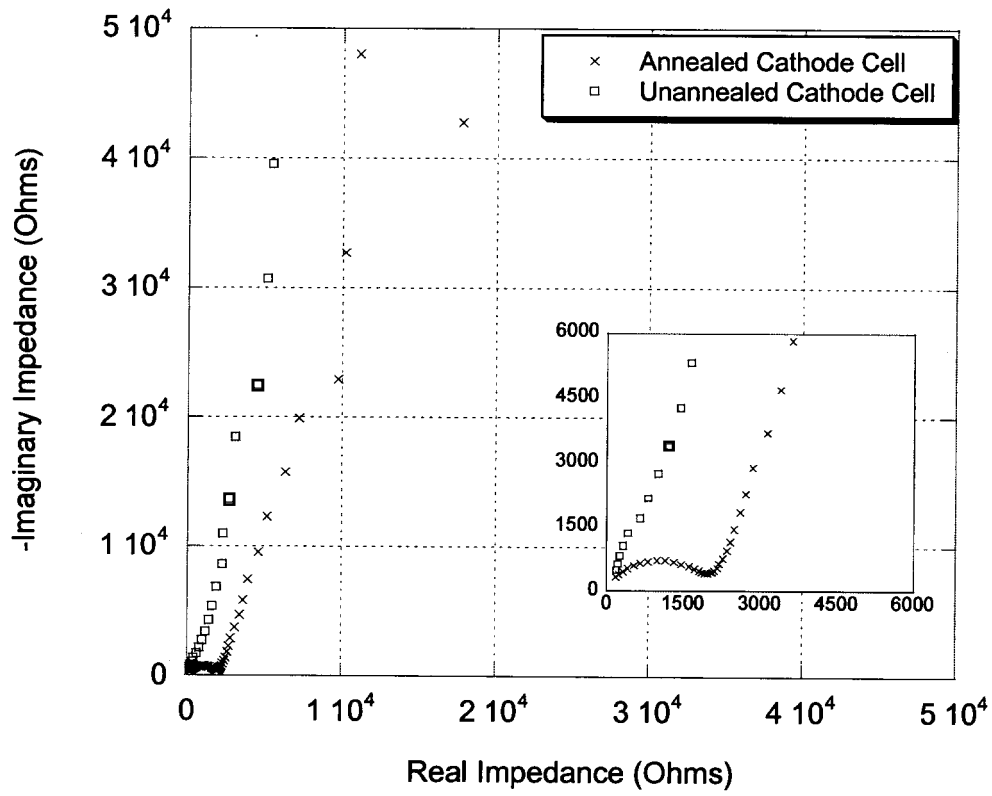


Fig. 14.

| Layer | Nominal Thickness (μm) | RF Power Density (W/in^2) | Deposition Pressure (mT) | Sputter Gas Composition |
|-----------------------------|-------------------------------------|---|--------------------------|-----------------------------|
| Ti adhesion | 0.05 | 42 | 10 | Ar |
| Pt current collector | 0.3 | 42 | 10 | Ar |
| LiCoPO ₄ cathode | 0.3 | 21 | 15 | 25% O ₂ , 75% Ar |
| LiPON electrolyte | 3.0 | 14 | 15 | N ₂ |
| Li anode | 5 | (thermally evaporated) | -- | -- |

Table 1

| Cell voltage (V) | CPE(int) | | CPE(el) | | R(el) | CPE(rxn) | | R(rxn) | CPE(cath) | | R(cath) | C(g) |
|---------------------|----------|-------|---------|-------|-------|----------|---------|---------|-----------|---------|---------|--------|
| | T | P | T | P | | T | P | | T | P | | |
| Pt LiPON Li: | | | | | | | | | | | | |
| 0.55 | 5.62E-5 | 0.966 | 3.76E-7 | 0.661 | 2290 | 1.20E-5 | 8.67E-1 | 184 | -- | -- | -- | 1.00E- |
| 2.8 | 1.93E-4 | 0.676 | 3.75E-7 | 0.661 | 2150 | 1.20E-5 | 8.67E-1 | 4321 | 3.83E-6 | 6.69E-1 | 4.09E+4 | 1.99E- |
| 2.5 | 1.37E-3 | 0.595 | 3.75E-7 | 0.661 | 2220 | 1.20E-5 | 8.67E-1 | 184 | 3.16E-4 | 6.69E-1 | 2.10E+4 | 1.83E- |
| 2.25 | 5.37E-5 | 0.75 | 3.75E-7 | 0.661 | 2520 | 1.20E-5 | 8.67E-1 | 8.78E+4 | 3.83E-6 | 6.69E-1 | 1.53E+5 | 1.99E- |
| 3 | 6.64E-5 | 0.75 | 3.75E-7 | 0.661 | 2030 | 7.60E-6 | 8.67E-1 | 6.60E+5 | 3.83E-6 | 6.69E-1 | 1.68E+6 | 1.99E- |
| 3.25 | 4.11E-5 | 0.75 | 3.75E-7 | 0.661 | 2180 | 7.63E-6 | 8.67E-1 | 2.00E+6 | 1.38E-6 | 6.69E-1 | 5.05E+6 | 5.14E- |
| 3.6 | 1.02E-4 | 0.75 | 3.75E-7 | 0.661 | 2170 | 5.40E-6 | 8.67E-1 | 2.00E+6 | 1.38E-6 | 6.69E-1 | 5.08E+6 | 2.00E- |

Table 2.